STRUCTURAL BIOLOGY COMMUNICATIONS

ISSN 2053-230X

Received 18 July 2020
Accepted 18 October 2020

Edited by J. Agirre, University of York, United Kingdom

Keywords: chitin; chitoporin; outer membrane proteins; *Serratia marcescens*; sugar transport; chitoligosaccharides; sugar-specific porins.

Chitoporin from *Serratia marcescens*: recombinant expression, purification and crystallization

Rawiporn Amornloetwattana,[a] Robert C. Robinson,[a,b] Hannadige Sasimali Madusanka Soysa,[c] Bert van den Berg[d] and Wipa Suginta[a]*

[a]School of Biomolecular Science and Engineering, Vidyasirimedhi Institute of Science and Technology, Payupnai, Wangchan, Rayong 21210, Thailand, [b]Research Institute for Interdisciplinary Science, Okayama University, Okayama 700-8530, Japan, [c]Department of Physical Sciences and Technology, Faculty of Applied Sciences, Sabaragamuwa University of Sri Lanka, Belihuloya 70140, Sri Lanka, and [d]Biosciences Institute, The Medical School, Newcastle University, Newcastle upon Tyne NE2 4HH, United Kingdom. *Correspondence e-mail: wipa.s@vistec.ac.th

Serratia marcescens is an opportunistic pathogen that commonly causes hospital-acquired infections and can utilize chitin-enriched nutrients as an alternative energy source. This study reports the identification of a chitoporin (ChiP), termed *Sm*ChiP, from the outer membrane of *S. marcescens*. Sequence alignment with genetically characterized ChiPs suggests that *Sm*ChiP is more closely related to the monomeric *Ec*ChiP from *Escherichia coli* than to the trimeric *Vh*ChiP from *Vibrio campbellii*. A single crystal of *Sm*ChiP grown under the condition 22%(*w*/*v*) PEG 8000, 0.1 *M* calcium acetate, 0.1 *M* MES pH 6.0 diffracted X-ray synchrotron radiation to 1.85 Å resolution. *Sm*ChiP co-crystallized with chitohexaose under the condition 19%(*w*/*v*) PEG 1500, 2 *M* ammonium phosphate monobasic, 0.1 *M* HEPES pH 7.0 diffracted X-rays to 2.70 Å resolution. Preliminary crystallographic analysis shows that both *Sm*ChiP crystal forms contain one molecule per asymmetric unit and that they belong to the tetragonal space groups $P4_22_12$ and $P4_12_12$, respectively. The *Sm*ChiP crystal has unit-cell parameters $a = 82.97$, $b = 82.97$, $c = 189.53$ Å, $\alpha = \beta = \gamma = 90^\circ$, while the crystal of *Sm*ChiP in complex with chitohexaose has unit-cell parameters $a = 73.24$, $b = 73.24$, $c = 213.46$ Å, $\alpha = \beta = \gamma = 90^\circ$. Initial assessment of the complex structure clearly revealed electron density for the sugar ligand. Structure determination of *Sm*ChiP in the absence and presence of chitohexaose should reveal the molecular basis of chitin utilization by *S. marcescens*.

1. Introduction

Serratia marcescens is a species of Gram-negative, facultative bacteria that belongs to the family Enterobacteriaceae (Golemi-Kotra, 2008; Hejazi & Falkiner, 1997). It has a widespread occurrence in different settings, such as in soil, water, plants and the digestive tracts of animals and humans (Hejazi & Falkiner, 1997; Mahlen, 2011). Several strains of *S. marcescens* have been identified as opportunistic pathogens that cause urinary-tract, bloodstream and respiratory-tract infections in hospitalized adults, and in the gastrointestinal systems of children (Golemi-Kotra, 2008; Gupta *et al.*, 2014; Hejazi & Falkiner, 1997; Mahlen, 2011). *S. marcescens* species usually grow on various organic materials and starchy surfaces by secreting several hydrolytic enzymes that degrade polymeric biomolecules, such as DNases, gelatinases, lipases and proteases. They also secrete several chitinolytic enzymes, such as ChiA, ChiB, ChiC, ChiD (Cabib, 1988; Młynarczyk *et al.*, 2007; Monreal & Reese, 1969; Vaaje-Kolstad *et al.*, 2013) and

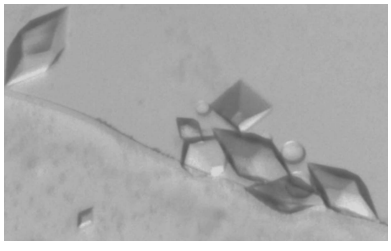

chitin-binding protein (CBP21; Vaaje-Kolstad *et al.*, 2005), which allow them to utilize chitinous materials as alternative sources of carbon and nitrogen. Despite the expression of these well characterized chitin-degrading enzymes and chitin-binding protein, there is only scarce evidence on how the chitin-degradation products (chitooligosaccharides) are taken up through the outer membrane (OM) of *S. marcescens*. A chitoligoosaccharide-specific porin (ChiP) was first described in a marine *Vibrio* species (Keyhani *et al.*, 2000). The wild-type *V. furnissii* expressing ChiP could grow on minimal medium containing $(GlcNAc)_{2,3}$ and could take up these chitooligosaccharides, while the ChiP-null mutant showed a drastic decrease in the rate of cell growth and chitooligosaccharide uptake.

Detailed functional characterization of *Vh*ChiP from *V. campbellii* (formerly *V. harveyi*) type strain BAA-1116 has been reported, including pore-forming properties (Suginta, Chumjan, Mahendran, Janning *et al.*, 2013), sugar specificity (Suginta, Chumjan, Mahendran, Schulte *et al.*, 2013) and statistical analysis of chitooligosaccharide transport (Suginta, Khunkaewla *et al.*, 2013). When reconstituted into artificial phospholipid bilayers, *Vh*ChiP facilitates ion flow with an average conductance of 1.8 nS and is highly responsive to exposure to long-chain chitooligosaccharides, with chitohexaose being the most preferred substrate (Suginta, Chumjan, Mahendran, Janning *et al.*, 2013). The crystal structures of OM-expressed (PDB entry 5mdq) and *in vitro* folded *Vh*ChiP (PDB entry 5mdo) have been reported at resolutions of 1.95 and 2.5 Å, respectively (Aunkham *et al.*, 2018). The *Vh*ChiP structure is a trimeric assembly, with each monomeric subunit containing a 16-stranded β-barrel and an N-terminal periplasmic sequence (the so-called N-plug) that is believed to regulate the open and closed states of the channel. Structures of *Vh*ChiP in complex with chitotetraose (PDB entry 5mds) and chitohexaose (PDB entry 5mdr) were also solved at resolutions of 2.6 and 1.9 Å, respectively. The sugar ligand was contained inside the protein lumen; the pore-lining residues formed a large hydrogen-bond network with the sugar side chains, while some surface-exposed aromatic residues formed hydrophobic interactions with the pyranose rings of the bound sugar. Stochastic analysis of ion currents in the presence of chitohexaose suggested that sugar translocation is likely to be achieved through correlated trapping/untrapping dynamics, causing transient movements along the sugar passage inside the long, narrow channel (Suginta & Smith, 2013; Suginta *et al.*, 2016).

A different class of ChiPs has been also documented. We previously identified a quiescent *chiP* gene encoding *Ec*ChiP from the genome of *Escherichia coli* strain K-12 substrain MG1655 (Soysa & Suginta, 2016). The *chiP* gene was cloned into pET-23d(+) expression vector, which could be expressed in the Omp-deficient *E. coli* BL21 (Omp8) strain. Unlike *Vh*ChiP, which is an OmpC-like channel that consists of three identical subunits (Suginta, Chumjan, Mahendran, Janning *et al.*, 2013) and has exceptional specificity towards long-chain chitooligosaccharides (Suginta, Chumjan, Mahendran, Schulte *et al.*, 2013), the recombinant *Ec*ChiP was characterized as a monomeric OprD-like porin with a molecular weight of ~52 kDa and showed only 12% sequence identity to *Vh*ChiP. *Ec*ChiP could form a stable channel and could fully conduct ion flows with an average single-channel conductance of 0.5 nS (Soysa *et al.*, 2017, 2018). Nevertheless, it exhibited a significantly lower affinity towards chitooligosaccharides, with the binding constant towards the most preferred substrate being tenfold lower than that of *Vh*ChiP (Soysa *et al.*, 2017). In further relevant studies, the *chiP* gene encoding *Sm*ChiP from *S. marcescens* 2170 was identified to be part of the *ybfMN-ctp* cluster (Toratani *et al.*, 2012). This gene cluster has subsequently been referred to as the *chiPQ-ctb* cluster (Takanao *et al.*, 2014). Cell growth has been reported to be affected in *S. marcescens* mutants with deletions of the *chiP*, *chiX* and *chiQ* genes. In particular, the Δ*chiP* mutant showed a significantly lower ability to grow on media supplemented with colloidal chitin and chitobiose, and showed no growth on media containing chitotriose. Subsequent studies demonstrated that the *chiX* small RNA controls the expression of chitin-degrading enzymes (chitinases and chitobiase), a chitin-binding protein (CBP21) and a chitooligosaccharide transporter (ChiP) (Toratani *et al.*, 2012; Suzuki *et al.*, 2016). Nevertheless, no detailed functional and structural characterization of chitin acquisition by *Sm*ChiP has been performed to date. This short communication describes the gene identification, gene synthesis, recombinant expression, purification and crystallization of *Sm*ChiP expressed in *E. coli*. Crystallization of *Sm*ChiP in the absence and presence of a chitooligosaccharide substrate was successful, allowing high-quality crystallographic data for *Sm*ChiP and *Sm*ChiP in complex with chitooligosaccharide to be obtained. An initial sequence analysis suggested that *Sm*ChiP is similar to *Ec*ChiP, but differs from *Vh*ChiP. Therefore, structure determination will reveal the exclusive properties of *Sm*ChiP with respect to how it conducts ion currents and acquires sugar substrate.

2. Materials and methods

2.1. Recombinant expression, protein extraction and purification

AR325_08275, an ORF corresponding to a *chiP* gene in the genome of *S. marcescens*, was identified from the UniProtNK database (https://www.uniprot.org/uniprot/A0A0P0QBS3). The *Serratia chiP* gene fragment containing 1416 base pairs was synthesized by GenScript and cloned into pET-23a(+) using BamHI/XhoI restriction sites. The gene construct, termed pET-23a(+)_*Serratia chiP*, was transformed into Omp-deficient *E. coli* BL21 (Omp8) Rosetta host cells and the overnight culture of transformed cells was transferred to Luria–Bertani broth containing 100 μg ml^{-1} ampicillin and 25 μg ml^{-1} kanamycin and grown at 300 K. During the exponential growth phase (OD_{600} of ~0.6–0.8), *Sm*ChiP expression was induced with 0.5 m*M* (final concentration) isopropyl β-D-1-thiogalactopyranoside. After 6 h of further incubation at 300 K, the cell pellet was harvested by centrifugation at 2590*g* for 30 min at 277 K.

To extract and purify *Sm*ChiP, the cell pellet was resuspended in lysis buffer (20 m*M* Tris–HCl pH 8.0, 2.5 m*M* $MgCl_2$, 0.1 m*M* $CaCl_2$) containing 0.1%(*v*/*v*) Triton X-100, 10 µg ml^{-1} RNase A and 10 µg ml^{-1} DNase I. Cells were disrupted on ice with a high-speed ultrasonic processor (Cole-Parmer, Vernon Hills, Illinois, USA) for 10 min; 2%(*w*/*v*) SDS was then added to the cell suspension, which was further incubated at 323 K for 60 min using a Thermomixer Comfort (Eppendorf AG, Hamburg, Germany) with a thermoblock in 4 × 50 ml Falcon tubes to ensure complete lysis. Cell-wall components were removed by ultracentrifugation at 35 000*g* at 277 K for 45 min. The pale pellet containing the membrane fraction and recombinant *Sm*ChiP was extracted twice with 2.5%(*v*/*v*) *n*-octylpolyoxyethylene (octyl-POE; Alexis Biochemicals, Lausanne, Switzerland) in 10 m*M* HEPES buffer pH 7.5, 100 m*M* NaCl using a homogenizer. The suspension was incubated at 300 K with gentle shaking for 1 h using the Thermomixer and the supernatant containing solubilized *Sm*ChiP was then collected by ultracentrifugation at 115 600*g* for 1 h. The supernatant was concentrated, and the detergent was exchanged to 0.2%(*v*/*v*) lauryldimethylamine oxide (LDAO; Sigma–Aldrich, Singapore) using an Amicon concentrator (10 kDa molecular-weight cutoff; Merck Millipore, Tullagreen, Cork, Ireland). *Sm*ChiP was further purified to homogeneity by size-exclusion chromatography using a Sephacryl S-200 HR 26/100 column connected to an ÄKTA pure FPLC (GE Healthcare Bio-Sciences, Uppsala, Sweden), with a flow rate of 1.0 ml min^{-1}. The purity of the *Sm*ChiP peak from the size-exclusion step was verified by SDS–PAGE, the fractions containing highly purified *Sm*ChiP were pooled and the buffer was exchanged to 10 m*M* HEPES pH 7.4 containing 100 m*M* LiCl, 0.4%(*w*/*v*) tetraethylene glycol monooctyl ether (C8E4; Anatrace, Maumee, Ohio, USA) in an Amicon concentrator as described above. The protein concentration was estimated from A_{280} using a molar extinction coefficient of 126 170 M^{-1} cm^{-1}. The freshly prepared sample (15.0 mg ml^{-1}) was used to set up crystallization screens, while the remaining sample was aliquoted into small volumes, snap-frozen in liquid nitrogen and immediately stored at 193 K for further use. Detergent extraction and purification of *Sm*ChiP for the purposes of co-crystallization were carried out separately following the protocol described above, except that the protein was buffer-exchanged into 10 m*M* HEPES pH 7.4 containing 100 m*M* LiCl and 0.4%(*v*/*v*) C8E4 using an Amicon concentrator for crystallization trials. The molecular weight of *Sm*ChiP was confirmed by electrospray mass-spectrometry analysis (First BASE Laboratories, Selangor Darul Ehsan, Malaysia).

2.2. Protein crystallization and data collection

Sitting-drop crystallization screening was carried out in Swissci 96-Well 2-Drop MRC Crystallization Plates (Molecular Dimensions, Sheffield, UK) using a Mosquito crystallization robot (TTP Labtech, Melbourn, UK). For crystallization trials of *Sm*ChiP, the freshly prepared protein (9.0 mg ml^{-1}) was screened using the MemGold and MemGold2 screening kits (Molecular Dimensions) with protein solution:mother liquor ratios of 200 nl:200 nl in the top wells and 200 nl:150 nl in the bottom wells. The screening plates were sealed immediately and incubated at 293 K. The appearance of single crystals was observed daily under a stereo microscope. Conditions that yielded single crystals were further optimized in 24-well plates using the hanging-drop vapour-diffusion method. In each well, two drops with different protein:precipitant volume ratios, 1.0 µl:1.0 µl and 1.5 µl:1.0 µl, were set up on an 18 mm cover slip. The crystallization plates were incubated at 293 K. Single crystals obtained from the optimized condition were harvested with nylon loops and plunged into liquid nitrogen using 20%(*w*/*v*) PEG 400 added to the mother liquor as a cryoprotectant and were tested for X-ray diffraction. For *Sm*ChiP in complex with chitooligosaccharide, the freshly prepared protein (15 mg ml^{-1}) dissolved in 10 m*M* HEPES pH 7.4 containing 100 m*M* LiCl and 0.4%(*v*/*v*) C8E4 was mixed with 10 m*M* chitohexaose prior to crystallization. The protein mixed with chitohexaose was incubated for 1 h before setting up crystallization screening. Initial screening and optimization were carried out using the MemTrans and MemChannel screening kits (Molecular Dimensions), with protein solution:mother liquor ratios of 150 nl:150 nl in the top well and 150 nl:200 nl in the bottom well, as described for *Sm*ChiP. The screening plates were incubated at 292 K. A hit condition with a large number of single crystals was optimized in 24-well plates using the hanging-drop method as for *Sm*ChiP. At this point, the protein:precipitant volume ratios were changed to 0.5 µl:0.5 µl and 0.5 µl:1.0 µl and the drops were incubated at 292 K. The single crystals from the optimized condition were harvested under a liquid-nitrogen steam as for *Sm*ChiP.

2.3. X-ray data collection and processing

X-ray diffraction data were collected from the *Sm*ChiP crystals on beamline I04-1 at Diamond Light Source (DLS), Didcot, UK. The data set was processed with *DIALS* and scaled with *AIMLESS* (Evans & Murshudov, 2013; Winter *et al.*, 2018). X-ray diffraction data from *Sm*ChiP in complex with chitohexaose were collected on beamline TPS 05A at the National Synchrotron Radiation Research Centre (NSRRC), Hsinchu, Taiwan. One data set was collected with 94.9% completeness and was indexed by *iMosflm* (Battye *et al.*, 2011). X-ray data scaling was performed by *AIMLESS*, which is available in the *CCP*4 package (Winn *et al.*, 2011).

3. Results and discussion

3.1. Identification of the *chiP* gene, gene synthesis and sequence analysis

The full-length *chiP* gene was identified from the UniProtKB Protein Database (UniProtKB entry A0A0P0QBS3). The *Serratia_chiP* gene construct encodes *Sm*ChiP that includes two extra amino acids GS from the BamHI cloning site and the 27-amino-acid signal sequence, followed by the mature *Sm*ChiP polypeptide of 435 amino

acids. The predicted molecular weight of mature *Sm*ChiP was 48 987 Da and the pI was 5.07. Multiple sequence alignment of *Sm*ChiP with two other functionally characterized ChiPs, *Ec*ChiP from *E. coli* (Soysa & Suginta, 2016; Soysa *et al.*, 2017, 2018) and *Vh*ChiP from *V. campbellii* (formerly *V. harveyi*; Suginta, Chumjan, Mahendran, Janning *et al.*, 2013), gave 77% and 18% sequence identity to *Ec*ChiP and *Vh*ChiP, respectively (Fig. 1). This result indicated that *Sm*ChiP is likely to be closely related, both structurally and functionally, to *Ec*ChiP.

The amino-acid sequences of *Sm*ChiP and *Ec*ChiP are relatively different from that of *Vh*ChiP, with 45 amino-acid residues (highlighted in blue) that are completely conserved and distributed throughout the entire sequences. These conserved residues are presumed to participate in critical architectural features of the three porins but are not involved in sugar transport. It is notable that except for Asp135, none of the amino-acid residues (indicated with red circles) that interact with the substrate in *Vh*ChiP are found in *Ec*ChiP or *Sm*ChiP. However, these residues are identical in the latter two channels. Such differences within the interior of the channel may give rise to a different binding mode and substrate specificity of the monomeric *Sm*ChiP/*Ec*ChiP *versus* the trimeric *Vh*ChiP.

3.2. Protein expression, purification and mass determination

Recombinant *Sm*ChiP containing its own signal peptide was successfully expressed in the OM of the Omp-deficient *E. coli* (Omp8) Rosetta host. After cell lysis, the *Sm*ChiP-containing OM fraction was prepared by extraction with SDS followed by octyl-POE. At this stage, *Sm*ChiP with 70–80% purity was usually obtained. The protein was then purified to homogeneity by size-exclusion chromatography for crystallization trials. Fig. 2(*a*) shows a representative elution profile of *Sm*ChiP purified by HiPrep 16/100 Sephacryl S-200 HR column chromatography (upper panel), yielding a single peak in A_{280} with no peak corresponding to aggregated protein. The peak contained a major protein that migrated with an apparent molecular weight of approximately 45 kDa on SDS–PAGE (Fig. 2*a*, lower panel). We then performed thermal denaturation to identify the monomeric/oligomeric state of *Sm*ChiP. It is known that outer membrane porins are

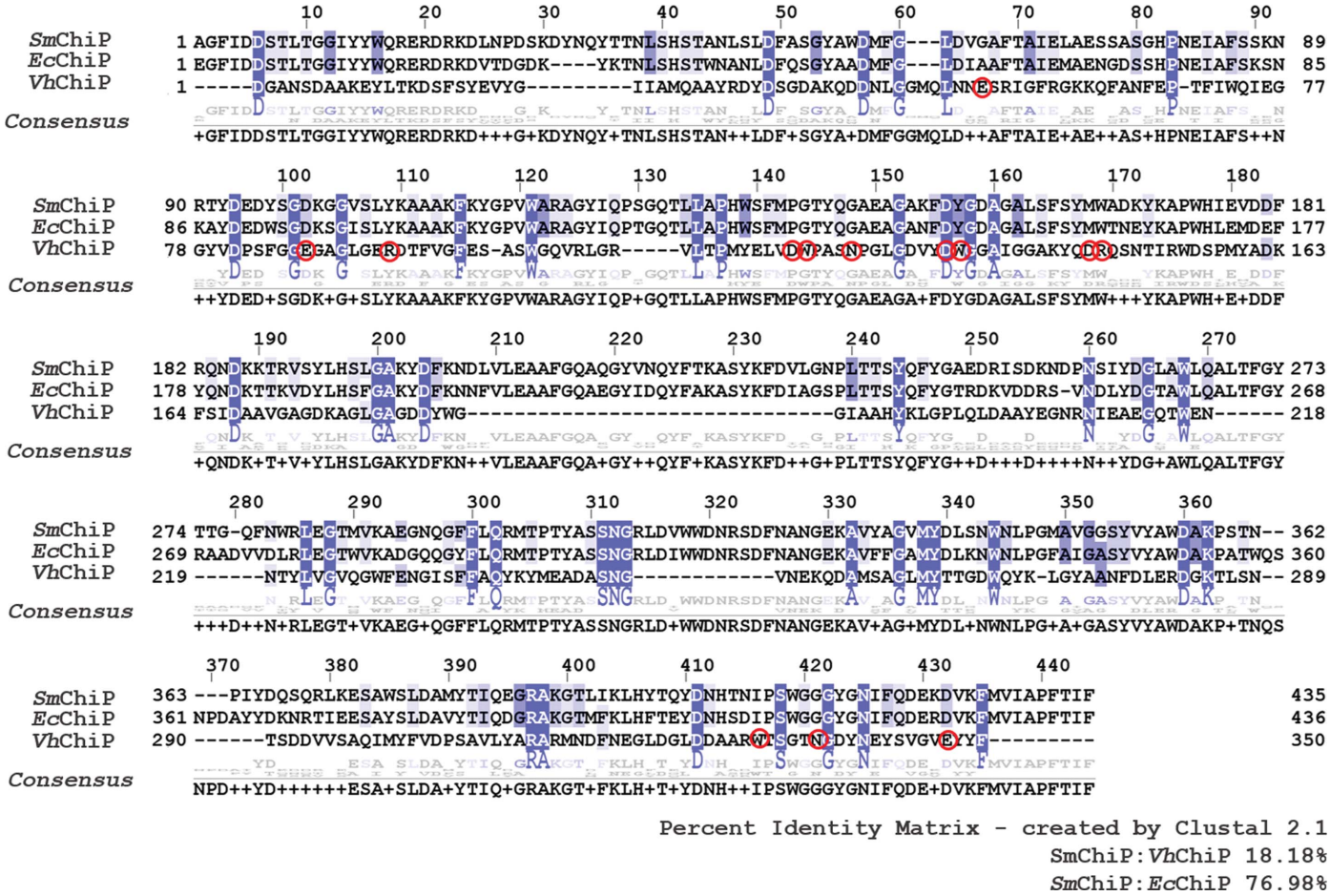

Figure 1
Multiple sequence alignment of *Sm*ChiP from *S. marcescens* (UniProtKB entry A0A0P0QBS3, this study) with *Ec*ChiP from *E. coli* (UniProtKB entry P75733) and *Vh*ChiP from *V. campbellii* (UniProtKB entry L0RVU0). The sequence alignment was generated by *Clustal* 2.1 and displayed by *Jalview* version 2.11.1.0. Blue shades indicate strictly conserved amino acids and red circles the amino-acid residues of *Vh*ChiP that bind to chitohexaose (Aunkham *et al.*, 2018).

structurally resistant to SDS treatment at room temperature, but unfold at high temperature (Reid *et al.*, 1988; Noinaj *et al.*, 2015). Fig. 2(*b*) shows the thermal dissociation of *Sm*ChiP. The protein was found to migrate at a position of about 45 kDa on SDS–PAGE after heating at 373 K for 10 min, while the unheated protein, corresponding to the folded protein, migrated at a position of about 35 kDa (Fig. 2*b*). The folded protein moved faster on SDS–PAGE, owing to its compact barrel structure, compared with the unfolded *Sm*ChiP. Similar results were observed with the monomeric *E. coli* chitoporin (*Ec*ChiP), which consists of one subunit of molecular weight 50 kDa (Soysa & Suginta, 2016). This is in contrast to the previous report on *Vh*ChiP from *V. campbellii* (formerly *V. harveyi*), where the folded protein migrated at a higher molecular weight under nondenatured conditions, while the unfolded protein appeared three times lower and was reported to be a trimeric protein (Soysa & Suginta, 2016; Aunkham *et al.*, 2018). Thus, the results obtained from thermal denaturation support the notion from multiple sequence alignment that *Sm*ChiP is more closely related to *Ec*ChiP than to *Vh*ChiP. The monomeric state of the purified protein was confirmed by intact mass analysis by ESI-LC mass spectrometry, which allows determination of the molecular weight with high precision. ESI-MS analysis of *Sm*ChiP is shown as individual spectra in Fig. 2(*c*), with the monoisotopic peaks in the ESI mass spectrum representing intact molecular species with variable charges. The vertical axis shows the relative abundances (intensities) of multiply charged species of *Sm*ChiP, and the horizontal axis represents the mass to charge ratio (m/z) of the multiply charged analyte. The intact mass of *Sm*ChiP was then determined by automated charge-state deconvolution to be 49 085 Da (inset in Fig. 2*c*), which is consistent within 0.2% standard error with the predicted theoretical mass of mature *Sm*ChiP (48 987 Da) as described earlier.

3.3. Crystallization and initial X-ray crystallographic analysis

Small single crystals of *Sm*ChiP were observed after one week in four conditions: conditions A8 [30%(*w*/*v*) PEG 400, 0.1 *M* $CdCl_2$, 0.1 *M* LiCl, 0.1 *M* sodium acetate pH 4.5] and D6 [26%(*v*/*v*) PEG 350 MME, 0.2 *M* $CaCl_2$ dihydrate, 0.1 *M* MES pH 6.5] from MemGold (designated MG1_A8 and MG1_D6, respectively) and conditions C10 [22%(*w*/*v*) PEG 8000, 0.1 *M*

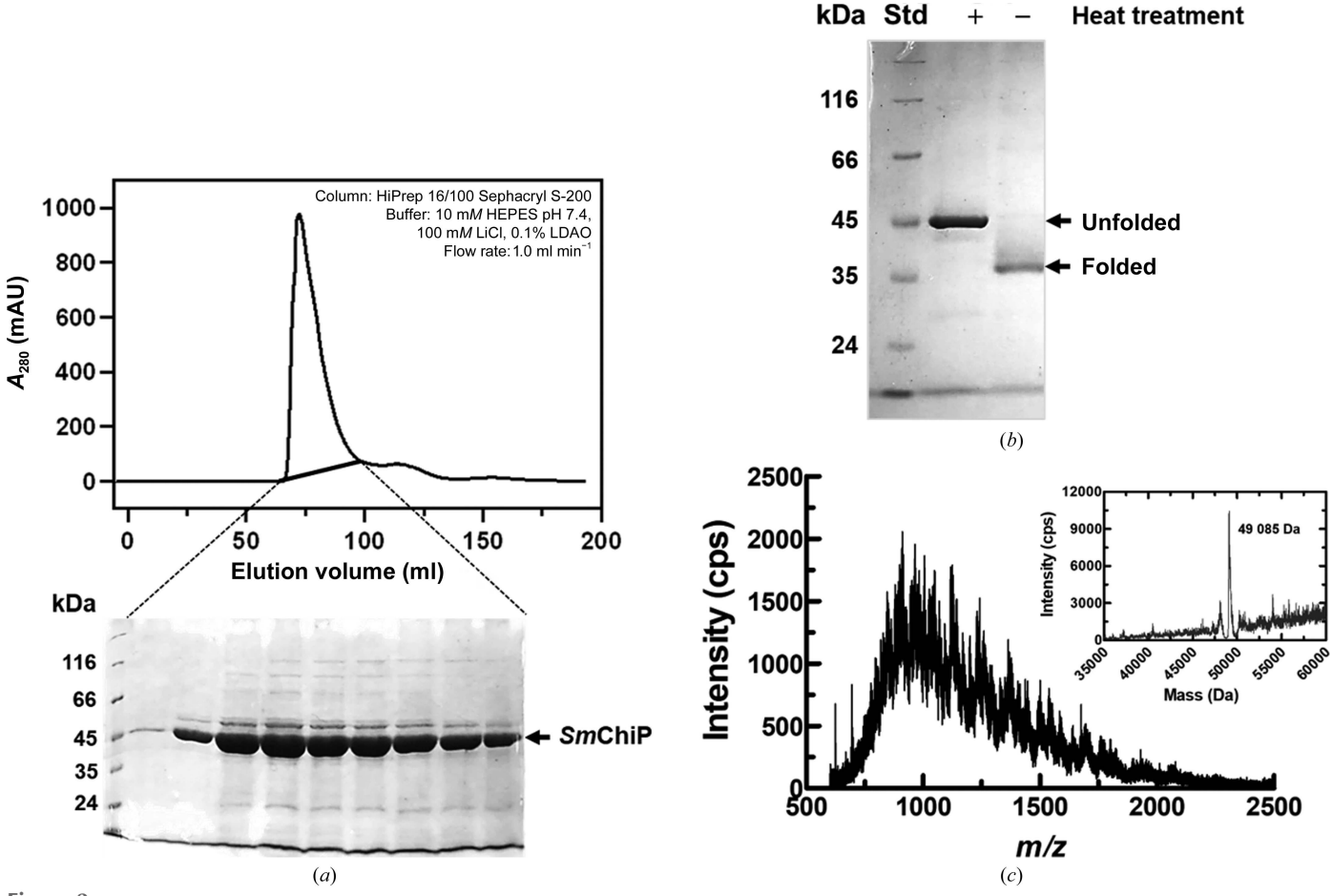

Figure 2
Preparation of *Sm*ChiP expressed in *E. coli*. (*a*) A representative elution profile of *Sm*ChiP eluted from a HiPrep 16/100 Sephacryl S-200 HR column with 10 m*M* HEPES pH 7.4, 100 m*M* LiCl, 0.1% LDAO (upper panel). SDS–PAGE showed that a single protein peak with an elution volume of 65–100 ml contained *Sm*ChiP as the major component (lower panel). (*b*) SDS–polyacrylamide gel showing migration of the purified *Sm*ChiP after heating at 373 K for 10 min (lane +) and without heat treatment (lane −). Lane Std contains molecular-weight markers (labelled in kDa). (*c*) Isotopic ionization pattern of *Sm*ChiP as determined by electrospray mass spectrometry. The inset shows the peak deconvolution.

Table 1
Crystallization conditions for *Sm*ChiP.

	*Sm*ChiP	*Sm*ChiP co-crystallized with chitohexaose
Screening		
Method	Sitting drop	Sitting drop
Temperature (K)	293	292
Protein concentration (mg ml^{-1})	9	15
Molar ratio of protein:ligand	—	0.3 m*M*:10 m*M*
Buffer composition	10 m*M* HEPES pH 7.5, 100 m*M* NaCl, 0.4%(*v*/*v*) C8E4	10 m*M* HEPES pH 7.4, 100 m*M* LiCl, 0.4%(*v*/*v*) C8E4
Condition composition	MG1_A8: 30%(*w*/*v*) PEG 400, 0.1 *M* $CdCl_2$, 0.1 *M* LiCl, 0.1 *M* sodium acetate pH 4.5 MG1_D6: 26%(*w*/*v*) PEG 350 MME, 0.2 *M* $CaCl_2$ dihydrate, 0.1 *M* MES pH 6.5 MG2_C10: 22%(*w*/*v*) PEG 8000, 0.1 *M* calcium acetate, 0.1 *M* MES pH 6.0 MG2_D12: 24%(*w*/*v*) PEG 400, 0.2 *M* calcium acetate, 0.1 *M* HEPES pH 7.0 MG2_D12: 24%(*w*/*v*) PEG 400, 0.2 *M* calcium acetate, 0.1 *M* HEPES pH 7.0	MT_F12: 38%(*w*/*v*) PEG 550 MME, 0.1 *M* $MgCl_2{\cdot}6H_2O$, 0.1 *M* Tris–HCl pH 8.7 MT_H12: 20%(*w*/*v*) PEG 1500, 0.2 *M* ammonium phosphate monobasic, 0.1 *M* HEPES pH 7.0
Volume and ratio of drop	400 nl, 1:1; 350 nl, 1.75:1	300 nl, 1:1; 350 nl, 1:1.75
Volume of reservoir (µl)	80	80
Optimization		
Method	Hanging drop	Hanging drop
Temperature (K)	293	292
Protein concentration (mg ml^{-1})	9	15
Molar ratio of *Sm*ChiP:chitohexaose	—	0.3 m*M*:10 m*M*
Buffer composition of protein solution	10 m*M* HEPES pH 7.5, 100 m*M* NaCl, 0.4%(*v*/*v*) C8E4	10 m*M* HEPES pH 7.4, 100 m*M* LiCl, 0.4%(*v*/*v*) C8E4
Condition composition	22%(*w*/*v*) PEG 8000, 0.1 *M* calcium acetate, 0.1 *M* MES pH 6.0 (from MG_C10)	19%(*w*/*v*) PEG 1500, 0.2 *M* ammonium phosphate monobasic 0.1 *M* HEPES pH 7.0 (from MT_H12)
Volume and ratio of drop	2 µl, 1:1; 2.5 µl, 1:1.15	1 µl, 1:1; 1.5 µl, 1:1.5
Volume of reservoir (µl)	300	300

calcium acetate, 0.1 *M* MES pH 6.0] and D12 [24%(*w*/*v*) PEG 400, 0.2 *M* calcium acetate, 0.1 *M* HEPES pH 7.0] from MemGold2 (designated MG2_C10 and MG2_D12, respectively). During co-crystallization, single crystals were observed within one week from conditions F12 [38%(*w*/*v*) PEG 550 MME, 0.1 *M* $MgCl_2$ hexahydrate, 0.1 *M* Tris–HCl pH 8.7] in both the top and bottom wells (1:1 and 1:1.75 protein:mother liquor ratios) and H12 [20%(*w*/*v*) PEG 1500, 0.2 *M* ammonium phosphate monobasic, 0.1 *M* HEPES pH 7.0] from MemTrans (designated MT_F12 and MT_H12, respectively). The initial hits were further optimized as described above and a summary of the crystallization conditions for *Sm*ChiP and co-crystallized *Sm*ChiP is given in Table 1.

Although several single hexagonal crystals of *Sm*ChiP were obtained from MG1_D6, the crystal dimensions were relatively small (approximately 20 × 30 µm; Fig. 3*a*), so this condition was not selected for further optimization and the crystals were not tested for X-ray diffraction. After hanging-drop optimization, good-sized and well defined hexagonal bipyramidal crystals (dimensions of about 50 × 100 µm) were observed after one day of incubation at 293 K in the optimized condition MG2_C10 (Fig. 3*b*). Crystals of *Sm*ChiP in complex with chitohexaose were successfully grown under the condition 19%(*w*/*v*) PEG 1500, 0.2 *M* ammonium phosphate monobasic, 0.1 *M* HEPES pH 7.0. Thin plate tetragonal crystals appeared after two days of incubation at 292 K, with dimensions of approximately 30 × 50 µm (Fig. 3*c*).

X-ray diffraction data were collected from the *Sm*ChiP crystals obtained under the optimized condition on beamline I04-1 at Diamond Light Source. The best data set was

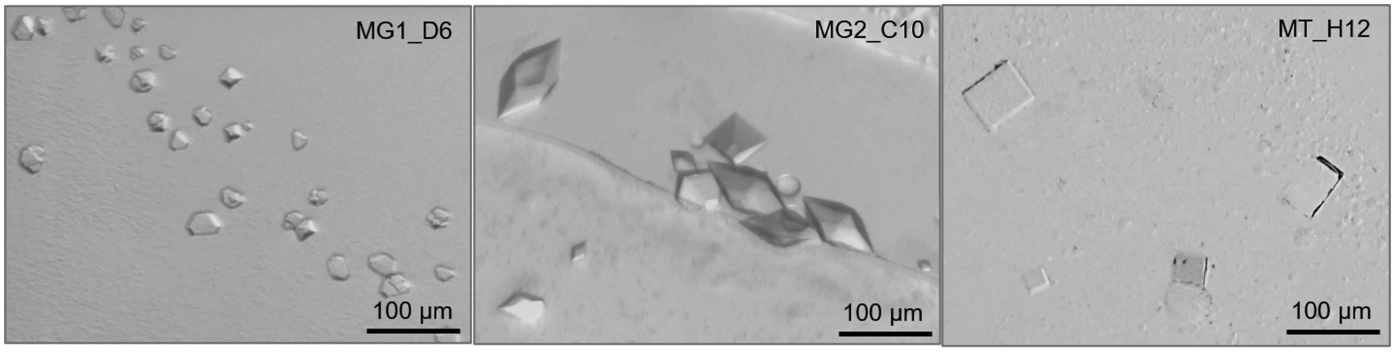

(*a*) (*b*) (*c*)

Figure 3
Single crystals of *Sm*ChiP. (*a*) Crystals of *Sm*ChiP obtained from the initial screen condition MG1_D6. (*b*) Crystals of *Sm*ChiP obtained from the optimized condition 22%(*w*/*v*) PEG 8000, 0.1 *M* calcium acetate, 0.1 *M* MES pH 6.0. (*c*) Crystals of *Sm*ChiP co-crystallized with chitohexaose from the optimized condition 19%(*w*/*v*) PEG 1500, 0.2 *M* ammonium phosphate monobasic, 0.1 *M* HEPES pH 7.0.

Table 2
Data-collection and processing statistics.

Values in parentheses are for the outer resolution shell.

	Apo *Sm*ChiP	*Sm*ChiP–chitohexaose
Resolution cutoff (Å)	1.85	2.70
Beamline	I04-1, DLS	TPS 05A, NSRRC
Wavelength (Å)	0.97886	0.99984
Resolution range (Å)	94.76–1.85 (1.89–1.85)	71.15–2.70 (2.83–2.70)
Space group	$P4_22_12$	$P4_12_12$
a, b, c (Å)	82.9, 82.97, 189.53	73.24, 73.24, 213.46
α, β, γ (°)	90, 90, 90	90, 90, 90
Total No. of reflections	800417	100353
No. of unique reflections	57273	15892
Completeness (%)	100 (94.5)	99.0 (94.9)
Multiplicity	11.7 (9.8)	6.3 (6.5)
Mean $I/\sigma(I)$†	24.8 (2.5)	8.7 (3.0)
R_{merge}‡	0.101 (0.903)	0.164 (0.922)
$CC_{1/2}$	0.993 (0.647)	0.966 (0.569)

† Mean $I/\sigma(I) = \langle\langle I_h\rangle/\sigma'(\langle I_h\rangle)\rangle$. ‡ $R_{merge} = \sum_{hkl}\sum_i |I_i(hkl) - \langle I(hkl)\rangle|/\sum_{hkl}\sum_i I_i(hkl)$, where $I_i(hkl)$ is the intensity of the ith measurement of an equivalent reflection with indices hkl.

collected with 100% completeness to a resolution of 1.85 Å (Fig. 4*a*). The *L*-test estimated a twinning fraction of 0.063, indicating no twinning problems. The crystal diffraction showed substantially low mosaicity and a single lattice, indicating the overall high quality of this data set. *POINTLESS* predicted $P4_22_12$ to be the most likely space group, with a space-group confidence of 0.91. The unit-cell parameters are a = 82.97, b = 82.97, c = 189.53 Å, $\alpha = \beta = \gamma = 90°$. The estimated Matthews coefficient of 3.33 Å^3 Da^{-1} suggested the presence of one molecule in the asymmetric unit and a solvent content of 63.1%.

The X-ray diffraction data for *Sm*ChiP in complex with chitohexaose were collected on beamline TPS 05A at the National Synchrotron Radiation Research Center (NSRRC), Taiwan. Data from a crystal grown under the condition 19%(*w*/*v*) PEG 1500, 0.2 *M* ammonium phosphate monobasic, 0.1 *M* HEPES pH 7.0 were collected to a resolution of 2.38 Å. Using the half-set correlation coefficient ($CC_{1/2}$) and $I/\sigma(I)$ criteria (Winn *et al.*, 2011) with the accepted values of $CC_{1/2}$ = 0.3 and $I/\sigma(I)$ = 1.0, the data were scaled to a resolution cutoff of 2.70 Å (Fig. 4*b*) with 94.9% completeness. The processed data have unit-cell parameters a = 73.24, b = 73.24, c = 213.46 Å, $\alpha = \beta = \gamma = 90°$, and a Matthews coefficient of 2.89 Å^3 Da^{-1} indicates one molecule per asymmetric unit (solvent content of 57%). The indexing statistics were compatible with the tetragonal space group $P4_12_12$. Data-quality assessment of the final MTZ file by *phenix.xtriage* (Liebschner *et al.*, 2019; Otwinowski & Minor, 1997) estimated the mean *Z*-score of ice rings to be 2.05, indicating that no ice rings were detected (Morris *et al.*, 2004). The distribution of $|L|$ values indicates a twin fraction of 0.0, suggesting no twinning problems (Padilla & Yeates, 2003). The preliminary crystallographic parameters of both *Sm*ChiP crystal forms are summarized in Table 2.

3.4. Future prospects for structure determination

Since the X-ray data set for *Sm*ChiP without ligand was the first to be collected, we attempted to determine it independently of the crystal complex. The model of *Sm*ChiP was built by molecular replacement (MR) using the crystal structure of unliganded *Ec*ChiP from *E. coli* (PDB entry not yet publicly available) as a template. Although the final model of *Sm*ChiP has still to be refined, the electron density was of sufficient quality for all 435 amino-acid residues to be visible in the $2F_o - F_c$ map contoured at a σ level of 1.0. The electron density for *Sm*ChiP in complex with chitohexaose gave an OMIT map with reasonable electron density, allowing all of

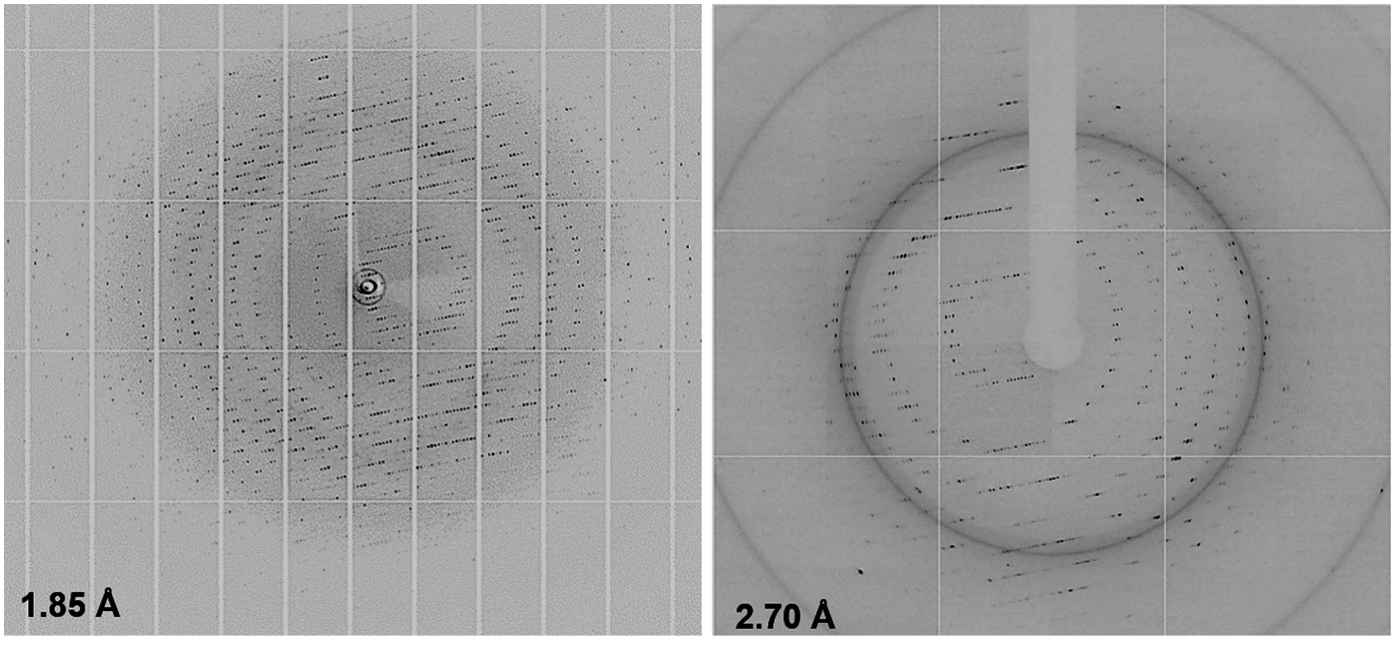

(*a*) (*b*)

Figure 4
High-resolution images of X-ray data from (*a*) *Sm*ChiP and (*b*) *Sm*ChiP in complex with chitohexaose.

the amino acids to be visualized. We observed clear electron density for four GlcNAc rings of chitohexaose in the middle of the protein pore, while partial electron densities for the GlcNAc rings at the termini of the sugar chain were seen owing to the high mobility of the sugar rings at the reducing and nonreducing ends of the sugar backbone. Refinement of both *Sm*ChiP models and structure validation are ongoing. Future research will examine the structural similarities and discrepancies between the monomeric *Sm*ChiP and the trimeric *Vh*ChiP in order to understand the molecular basis of sugar-channel interactions and chitooligosaccharide uptake by *S. marcescens*.

Acknowledgements

The authors declare no conflicts of interest. We thank the experimental facility and the technical services provided by the Synchrotron Radiation Protein Crystallography Facility of the National Core Facility Program for Biotechnology, Ministry of Science and Technology and the National Synchrotron Radiation Research Centre, a national user facility supported by the Ministry of Science and Technology, Taiwan, and Diamond Light Source, UK. We would like to thank Dr Yoshihito Kitaoku for assisting with data collection and processing, and Professor Takeshi Watanabe, Department of Applied Biological Chemistry, Niigata University, Japan for introducing the *chiP* gene from the *S. marcescens* system for functional characterization. We would like to thank Dr David Apps of the University of Edinburgh for critical reading and English improvement of the manuscript.

Funding information

WS received funding from Vidyasirimedhi Institute of Science and Technology (VISTEC) and the Thailand Research Fund (TRF) through a Basic Research Grant (Grant No. BRG610008). RA received a full-time MSc scholarship from VISTEC.

References

Aunkham, A., Zahn, M., Kesireddy, A., Pothula, K. R., Schulte, A., Baslé, A., Kleinekathöfer, U., Suginta, W. & van den Berg, B. (2018). *Nat. Commun.* **9**, 220.

Battye, T. G. G., Kontogiannis, L., Johnson, O., Powell, H. R. & Leslie, A. G. W. (2011). *Acta Cryst.* D**67**, 271–281.

Cabib, E. (1988). *Methods Enzymol.* **161**, 460–462.

Evans, P. R. & Murshudov, G. N. (2013). *Acta Cryst.* D**69**, 1204–1214.

Golemi-Kotra, D. (2008). *xPharm: The Comprehensive Pharmacology Reference*, edited by S. J. Enna & D. B. Bylund, pp. 1–6. New York: Elsevier.

Gupta, N., Hocevar, S. N., Moulton-Meissner, H. A., Stevens, K. M., McIntyre, M. G., Jensen, B., Kuhar, D. T., Noble-Wang, J. A., Schnatz, R. G., Becker, S. C., Kastango, E. S., Shehab, N. & Kallen, A. J. (2014). *Clin. Infect. Dis.* **59**, 1–8.

Hejazi, A. & Falkiner, F. R. (1997). *J. Med. Microbiol.* **46**, 903–912.

Keyhani, N. O., Li, X.-B. & Roseman, S. (2000). *J. Biol. Chem.* **275**, 33068–33076.

Liebschner, D., Afonine, P. V., Baker, M. L., Bunkóczi, G., Chen, V. B., Croll, T. I., Hintze, B., Hung, L.-W., Jain, S., McCoy, A. J., Moriarty, N. W., Oeffner, R. D., Poon, B. K., Prisant, M. G., Read, R. J., Richardson, J. S., Richardson, D. C., Sammito, M. D., Sobolev, O. V., Stockwell, D. H., Terwilliger, T. C., Urzhumtsev, A. G., Videau, L. L., Williams, C. J. & Adams, P. D. (2019). *Acta Cryst.* D**75**, 861–877.

Mahlen, S. D. (2011). *Clin. Microbiol. Rev.* **24**, 755–791.

Młynarczyk, A., Młynarczyk, G., Pupek, J., Bilewska, A., Kawecki, D., Łuczak, M., Gozdowska, J., Durlik, M., Pączek, L., Chmura, A. & Rowiński, W. (2007). *Transplant. Proc.* **39**, 2879–2882.

Monreal, J. & Reese, E. (1969). *Can. J. Microbiol.* **15**, 689–696.

Morris, R. J., Zwart, P. H., Cohen, S., Fernandez, F. J., Kakaris, M., Kirillova, O., Vonrhein, C., Perrakis, A. & Lamzin, V. S. (2004). *J. Synchrotron Rad.* **11**, 56–59.

Noinaj, N., Kuszak, A. J. & Buchanan, S. K. (2015). *Methods Mol. Biol.* **1329**, 51–56.

Otwinowski, Z. & Minor, W. (1997). *Methods Enzymol.* **276**, 307–326.

Padilla, J. E. & Yeates, T. O. (2003). *Acta Cryst.* D**59**, 1124–1130.

Reid, J., Fung, H., Gehring, K., Klebba, P. E. & Nikaido, H. (1988). *J. Biol. Chem.* **263**, 7753–7759.

Soysa, H. S. M. & Suginta, W. (2016). *J. Biol. Chem.* **291**, 13622–13633.

Soysa, H. S. M., Schulte, A. & Suginta, W. (2017). *J. Biol. Chem.* **292**, 19328–19337.

Soysa, H. S. M., Suginta, W., Moonsap, W. & Smith, M. F. (2018). *Phys. Rev. E*, **97**, 052417.

Suginta, W., Chumjan, W., Mahendran, K. R., Janning, P., Schulte, A. & Winterhalter, M. (2013). *PLoS One*, **8**, e55126.

Suginta, W., Chumjan, W., Mahendran, K. R., Schulte, A. & Winterhalter, M. (2013). *J. Biol. Chem.* **288**, 11038–11046.

Suginta, W., Khunkaewla, P. & Schulte, A. (2013). *Chem. Rev.* **113**, 5458–5479.

Suginta, W. & Smith, M. F. (2013). *Phys. Rev. Lett.* **110**, 238102.

Suginta, W., Winterhalter, M. & Smith, M. F. (2016). *Biochim. Biophys. Acta*, **1858**, 3032–3040.

Suzuki, K., Shimizu, M., Sasaki, N., Ogawa, C., Minami, H., Sugimoto, H. & Watanabe, T. (2016). *Biosci. Biotechnol. Biochem.* **80**, 376–385.

Takanao, S., Honma, S., Miura, T., Ogawa, C., Sugimoto, H., Suzuki, K. & Watanabe, T. (2014). *Biosci. Biotechnol. Biochem.* **78**, 524–532.

Toratani, T., Suzuki, K., Shimizu, M., Sugimoto, H. & Watanabe, T. (2012). *Biosci. Biotechnol. Biochem.* **76**, 1920–1924.

Vaaje-Kolstad, G., Horn, S. J., Sørlie, M. & Eijsink, V. G. (2013). *FEBS J.* **280**, 3028–3049.

Vaaje-Kolstad, G., Houston, D., Riemen, A., Eijsink, V. & van Aalten, D. (2005). *J. Biol. Chem.* **280**, 11313–11319.

Winn, M. D., Ballard, C. C., Cowtan, K. D., Dodson, E. J., Emsley, P., Evans, P. R., Keegan, R. M., Krissinel, E. B., Leslie, A. G. W., McCoy, A., McNicholas, S. J., Murshudov, G. N., Pannu, N. S., Potterton, E. A., Powell, H. R., Read, R. J., Vagin, A. & Wilson, K. S. (2011). *Acta Cryst.* D**67**, 235–242.

Winter, G., Waterman, D. G., Parkhurst, J. M., Brewster, A. S., Gildea, R. J., Gerstel, M., Fuentes-Montero, L., Vollmar, M., Michels-Clark, T., Young, I. D., Sauter, N. K. & Evans, G. (2018). *Acta Cryst.* D**74**, 85–97.